Available online at www.sciencedirect.com
SCIENCE DIRECT®
Journal of Nuclear Materials 337–339 (2005) 211–215
journal of nuclear materials
www.elsevier.com/locate/jnucmat

Angular dependence of energy and particle fluxes in a magnetized plasma

B. Koch *, W. Bohmeyer, G. Fussmann

Institut für Physik der Humboldt-Universität zu Berlin, AG Plasmaphysik, Humboldt-Universität zu Berlin, Newtonstr. 14 12489, Berlin, Germany

Abstract

A flat probe allowing simultaneous measurements of energy flux and current density as functions of a bias voltage was rotated in a spatially homogeneous plasma. The experiments were conducted at the PSI-2 facility, a linear divertor simulator with moderate magnetic field strength. Sheath parameters (ion current density j_i, floating potential U_f, energy flux density q, ion energy reflection coefficient R_E and sheath energy transmission coefficient γ) were determined as functions of the angle α between the probe surface normal and the magnetic field. A geometric model has been developed to explain the ion flux density at grazing incidence.

PACS: 52.40.Hf
Keywords: Plasma-wall interactions; Plasma sheath; Oblique magnetic field; Particle flux; Energy flux

1. Introduction

In fusion experiments the energy flux to the vessel walls and in particular to the target plates is an important issue. In order to reduce the heat load, the target surfaces are usually designed to intersect magnetic field lines at very shallow angles. In this paper we report on an experimental investigation of the angular dependencies of some quantities of interest, in particular current and energy flux densities.

In a magnetic field, charged particles are essentially restrained to move along the field lines. Accordingly, a geometric cosine dependence for particle fluxes to the surfaces is to be expected. The physics of the plasma sheath under oblique incidence has been the subject of intensive theoretical investigations for a long time [1–4]. It is, for example, a vital issue for the interpretation of data acquired by flush mounted probes [5–8]. However, most theoretical results can only be made available by numerical calculations.

2. Experimental setup

Our experiments were conducted at the PSI-2 plasma generator, a stationary high current arc discharge confined by an axial magnetic field ($B = 0.1\,\mathrm{T}$). The plasma is produced between a heated LaB_6 cathode and a hollow anode made from molybdenum [9]. Achievable plasma parameters range from about $10^{15}\cdots10^{19}\,\mathrm{m}^{-3}$ for the plasma density and up to about 30 eV for the electron temperature. Hall parameters are of the order $h_e = \omega_{ce}\tau_e \approx 10^5$ and $h_{H^+} \approx 10^2$ to $h_{Ar^+} \approx 1$.

* Corresponding author. Tel.: +49 30 2093 7544; fax: +49 30 2093 7549.
E-mail address: bernd.koch@physik.hu-berlin.de (B. Koch).

0022-3115/$ - see front matter © 2004 Elsevier B.V. All rights reserved.
doi:10.1016/j.jnucmat.2004.10.028

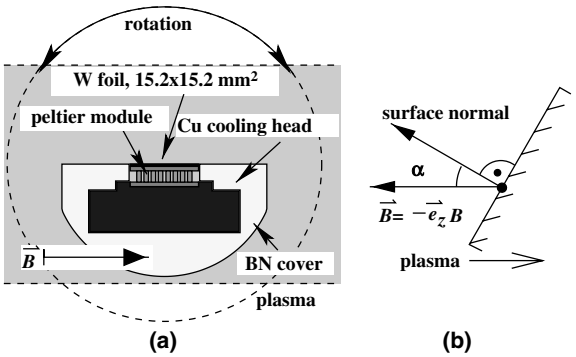

Fig. 1. Cut through the probe perpendicular to the axis of rotation (left) and definition of the angle α (right).

The measurements presented below were performed in the target chamber region by inserting a turnable flat probe (see Fig. 1) into the center of the plasma column. The probe head consists of a Peltier device on a water cooled base which is flush-mounted to a BN-ceramic cover. In the Peltier device the temperature difference between the plasma exposed surface and the base plate is proportional to the energy flux ($q \propto \Delta T$). Since ΔT can be measured with great accuracy and sensitivity, q is also determined with high precision ($\Delta q/q = 5\%$). The surface of the Peltier device is covered with a tungsten foil and can be biassed. The whole probe can be rotated automatically by a stepping motor with an angular resolution up to 0.01°. In order to reduce effects of plasma inhomogeneities the axis of rotation is located in the detector plane.

3. Experimental results

3.1. Probe characteristics at grazing incidence

At grazing incidence, $|\alpha| = 90°$, our rotating probe fairly resembles a flush mounted probe, a flat probe immersed in a limiter or divertor at a shallow angle with respect to the magnetic field. Foregoing experiments have shown very low ratios j_e^s/j_i^s, pronounced non-saturation of electron and ion currents and an overestimation of the electron temperature T_e [6,7]. Fig. 2 depicts two exemplary $j(U)$ characteristics obtained at grazing incidence of the magnetic field. One was measured with the probe head facing upward, $\alpha = +90°$, the other one for $\alpha = -90°$. Compared to the normal incidence case the current ratio j_e^s/j_i^s is very drastically reduced, from about $j_e^s/j_i^s \approx 24$ down to $j_e^s/j_i^s \approx 3$. This reduction, however, and the non-saturation as well are not symmetric with respect to α. Both effects are more pronounced for $\alpha = -90°$. By changing the sign of the magnetic field it could be confirmed that this asymmetry is related to the sense of gyration of the ions in combination with

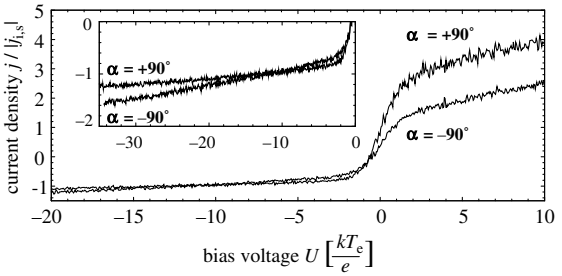

Fig. 2. $j(U)$ characteristics obtained at grazing incidence for $\alpha = \pm 90°$.

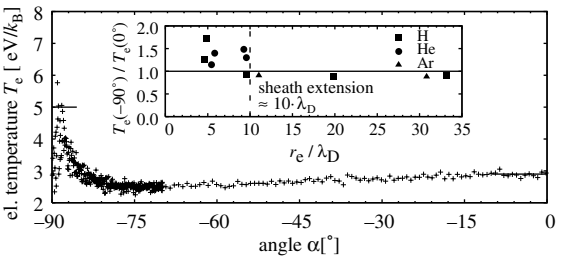

Fig. 3. T_e evaluated from $j(U)$ characteristics at different angles. The insert shows the relative T_e mismeasurement in dependence on r_e/λ_D for several ion species.

the geometry of the probe head: the asymmetry is interchanged when the magnetic field changes sign. Akin to the low ratio of j_e^s/j_i^s the floating potential is also reduced considerably for $|\alpha| \to 90°$ [10].

The overestimation of T_e is demonstrated in Fig. 3. It occurs when the electron gyro radius becomes comparable to the thickness of the Debye sheath, extending $5 \cdots 10 \cdot \lambda_D$. A possible explanation is an energy filtering effect which can be understood by applying the geometrical model, described later, to the electrons: Electrons with low energy, i.e. small gyro radii r_e and small velocity v_z, are lost before reaching the active area.

3.2. Determination of the ion energy reflection coefficient

For the evaluation of the $j(U) = j_i(U) + j_e(U)$ characteristics we choose a very common approach: for U below the plasma potential U_{pl}, the ion current density is a constant, the ion saturation current density j_i^s, plus a linear term $\propto U$ to account for non-saturation due to sheath expansion, $j_i(U) = C \cdot U + j_i^s$. For the electrons, an exponential rise is assumed, $j_e(U) = j_e^s \exp\left(-\frac{e[U-U_{pl}]}{kT_e}\right)$. Both, electrons and ions, also contribute to the total energy flux density $q(U) = q_i(U) + q_e(U)$. For the ions we have

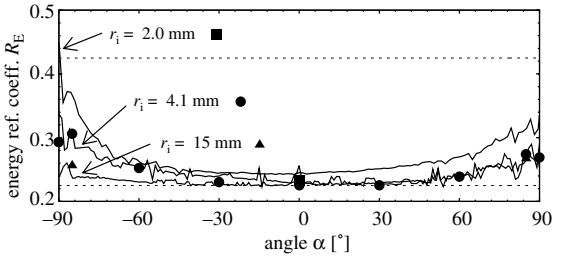

Fig. 4. Ion energy reflection coefficient $R_{i,E}(\alpha)$ for a hydrogen plasma.

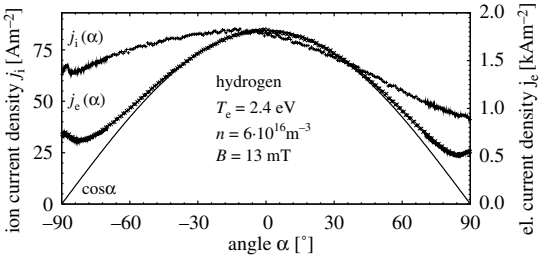

Fig. 5. Measured ion and electron saturation current densities.

$$q_i(U) = \left[[1 - R_{i,E}] \frac{5}{2} kT_i + e \mid U - U_{pl} \mid [1 - R_{i,E}] + E_{ion} - W \right] \frac{\mid j_i(U) \mid}{e}. \quad (1)$$

In this equation, the first line is due to the kinetic energy of the ions. $R_{i,E}$ is the ion energy reflection coefficient. The second line comprises the energy released during the recombination process with the ionization energy E_{ion} and the work function W. The electron contribution

$$q_e(U) = [2kT_e - e \mid U - U_{pl} \mid \delta_e + [1 - \delta_e]W] \frac{\mid j_e(U) \mid}{e} \quad (2)$$

includes the kinetic energy and the energy released when the electrons enter the conduction band of the surface material. δ_e is the secondary electron emission coefficient. By simultaneously fitting $j(U)$ and $q(U)$ to the experimental data, the ion energy reflection coefficient $R_{i,E}$ is obtained.

The results of the fitting procedure for a hydrogen plasma are given in Fig. 4. While, as expected, for large r_i, we observe only a negligible angular variation of $R_{i,E}$, for small r_i a sharp increase is found for $\alpha < 70°$ up to $R_{i,E}(-90°) \approx 2R_{i,E}(0°)$. The increase is not symmetric with respect to α due to the finite extension of the probe head along the axis of rotation.

3.3. Particle and Energy flux densities

Assuming ions and electrons strictly following the magnetic lines of force the angular dependence of the flux densities should show a cosine dependence: the flux densities parallel to the magnetic field remain constant and the projected area varies $\propto \cos(\alpha)$. However, looking at the measurements depicted in Fig. 5, considerable deviations from this behavior are noted.

In particular, the saturation current densities do not vanish for $|\alpha| \to 90°$. For the ions, this is in agreement with the basic model presented in Section 4. The angular asymmetry observed can be explained by extending the geometric model [11].

At shallow angles quite a surprising behavior is observed: approaching $|\alpha| \to 90°$, the experimental $j_i^s(\alpha)$ and $j_e^s(\alpha)$ exhibit a relative maximum. These peaks are most pronounced for small ion gyro radii, i.e. hydrogen ions at high magnetic field; they vanish completely in case of argon.

While the energy flux density is not shown here, it generally follows the particle flux dependence down to about $|\alpha| < 75°$. Beyond this, the influence of the magnetic field becomes apparent: a decrease of 50% in the normalized sheath energy transmission coefficient $\gamma := q/(T_e j_i^s)$ is observed. This strong decrease is caused by the reduction of the floating potential and an increase of the ion energy reflection coefficient.

4. A geometrical model

For the plasma parameters encountered in the experiments the extension of the Debye sheath is much smaller than the dimensions of the probe and it is also considerably smaller than the ion gyro radius. In order to determine the ion flux to the active area of the probe it is thus justified to disregard the effects of the electric field in a first order approach and to calculate the flux using the undisturbed gyro trajectories.

Fig. 6 sketches the probe geometry for grazing incidence of the magnetic field $\vec{B}$. The z-axis is chosen parallel to $\vec{B}$. Instead of treating the individual ion

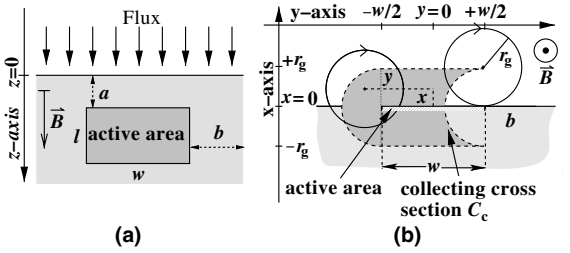

Fig. 6. Ion collection by a probe at grazing incidence. Only ions with guiding centers within the collecting cross-section are collected by the probe. Further restrictions are imposed by the relation of edge distance a, velocity v_z and gyro frequency ω_g.

trajectories we look at a set of ions with equal gyro radii r_i and a common guiding center (x, y) in the xy-plane. Evidently, only ions whose guiding center lie within the shaded area in Fig. 6, the collecting cross-section, can reach the active surface of the probe. Each particle must be weighted with the probability p of reaching the active area. At $z = 0$ the ions encounter the probe edge. Those ions which, at that moment, are located below the surface plane of the probe are lost immediately. The remaining ions are located on a circular arc of length $c = 2r_i \arccos\frac{-x}{r_i}$. They are deposited homogeneously within the region $0 \leqslant z \leqslant z_{max} = \frac{c}{2\pi r_i} s$ where $s = \frac{2\pi v_z}{\omega_g}$ is the distance covered within a gyration period. Three different cases are thus to be distinguished in the probability function

$$p(x, y, r_i, v_z) = 2\begin{cases} 0, & z_{max} < a, \\ \dfrac{z_{max} - a}{s}, & a \leqslant z_{max} \leqslant a + l, \\ \dfrac{l}{s}, & z_{max} > a + l, \end{cases} \tag{3}$$

where a factor 2 has been added to account for the symmetry in the z-direction. Integrating Eq. (3) over the collecting cross-section we obtain an effective collecting area depending on r_i and v_z only. Combining this with the ion velocity distribution function $f_0(r_i, v_z)$ yields the effective distribution function of the ions reaching the active area:

$$f_{eff}(r_i, v_z) = \frac{r_i}{\pi l}\underbrace{f_0(r_i, v_z)}_{\text{ivdf at } z=0} \times \begin{cases} 0, & s < a, \\ \pi - \dfrac{\pi a}{s} - \sin\dfrac{\pi a}{s}, & a \leqslant s \leqslant a + l, \\ \sin\dfrac{\pi[a + l]}{s} - \sin\dfrac{\pi a}{s} + \dfrac{\pi l}{s}, & s > a + l. \end{cases} \tag{4}$$

Apart from a global reduction, the maximum of the distribution function is shifted towards higher energies. Using Eq. (4) we can now calculate the ion flux to the active area. The results shown in Fig. 7, are in qualitative agreement with our measurements. The model thus successfully reflects the main features of the measurements.

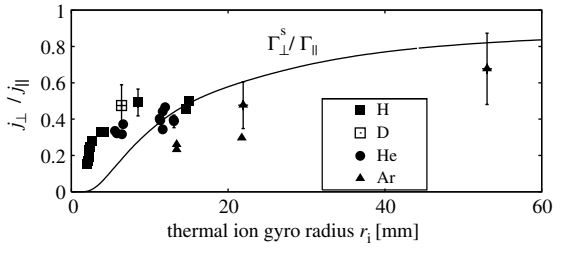

Fig. 7. Ratio of the ion saturation currents in comparison with modelling results based on Eq. (4). The geometry for the calculation was chosen according to the dimensions of the probe, $w = l = a = 15$ mm.

Accounting for the finite extension of the probe along the y-axis it is also possible to explain the asymmetry of j_i^s between $\alpha = -90°$ and $\alpha = +90°$. In this case, there can be an additional contribution from ions originating below the $x = 0$ plane beyond the edge of the probe. For example, if the ions are gyrating clockwise, the probe is infinite for $y < 0$ and has an edge at $y = w/2 + b$. There is then an additional contribution for $\alpha = +90°$ (probe facing in positive x-direction). However, the integration performed for (4) can now only be done numerically [11].

Similar considerations apply to the electrons. In this case we usually find $a \gg z_{max}$ and no electron flux is to be expected according to this model.

5. Summary and discussion

Measurements using a rotatable probe exhibit for $|\alpha| = 90°$ some interesting features. To some extend, those features are also pertinent for the application of flush mounted probes, e.g. a reduced ratio of j_e^s/j_i^s, non-saturation of electron and ion current density and an overestimation of the electron temperature are to be expected.

Under grazing incidence conditions, interesting effects are observed for the ion saturation part of the characteristic: First, the current does not saturate and second, there is an angular asymmetry. Non-saturation occurs only for one of the two grazing positions, at $\alpha = -90°$ for $B > 0$ and at $\alpha = +90°$ for $B < 0$. Although this effect cannot be explained in terms of the basic model presented in Section 4, we assume that this is due to the finite size of the probe.

The pseudo-increase of the electron temperature has been reproduced for small values of the ion gyro radius. It is suggested that this is caused by a deviation of the mean electron energy within the magnetized sheath. This deviation can be explained using the effective energy distribution function (4).

A strong deviation of the particle flux densities from a simple cosine dependence is observed. Considerable fractions of the ion and electron saturation current densities at normal incidence ($j_i^s(0°)$ and $j_e^s(0°)$) remain for $|\alpha| = 90°$. Moreover, a pronounced angular asymmetry has been found that (based on additional measurements not presented here) can be related to the magnetic field. Although there is no theory available to describe the proper behavior of $j_i^s(\alpha)$ and $j_e^s(\alpha)$, the ratio of $j_i^s(\pm 90°)/j_i^s(0°)$ can be reasonably explained by the simple model presented in Section 4. Quite surprisingly an increase of the particle flux density is observed when approaching grazing incidence conditions ($|\alpha| \to 90°$).

The energy flux density to the probe is explained invoking a basic model of the plasma sheath. The model allows us to determine experimentally the angular

dependence of one of the key parameters influencing the energy flux, the ion energy reflection coefficient $R_{i,E}$. A strong angular dependence was found for small values of the ion gyro radius r_i.

References

[1] P.C. Stangeby, The Plasma boundary of Magnetic Fusion Devices, IOP, 2000.
[2] R. Chodura, Phys. Fluids 25 (9) (1982) 1628.
[3] I.I. Beilis, M. Keidar, Phys. Plasmas 5 (5) (1998) 1545.
[4] U. Daybelge, B. Bein, Phys. Fluids 24 (6) (1981) 1190.
[5] A. Carlson, V. Rohde, M. Weinlich, J. Nucl. Mater. 241–243 (1997) 722.
[6] G.F. Matthews et al., Plasma Phys. Control. Fus. 32 (14) (1990) 1301.
[7] J.P. Gunn et al., Rev. Sci. Instrum. 66 (1) (1995) 154.
[8] U. Wolters, T. Daube, K.-U. Riemann, K. Wiesemann, Plasma Phys. Control. Fus. 41 (1999) 721.
[9] H. Behrend et al., in: Proc. 21st EPS Conf., 1994, p. 1328.
[10] B. Koch, W. Bohmeyer, G. Fussmann, J. Nucl. Mater. 313–316 (2003) 1114.
[11] B. Koch, Angular resolved measurements of particle and energy fluxes to surfaces in magnetized plasmas, PhD thesis, Humboldt-Universität zu Berlin.